

Collisionless absorption, hot electron generation, and energy scaling in intense laser-target interaction

T. Liseykina,^{1,2, a)} P. Mulser,³ and M. Murakami⁴

¹⁾*Institut für Physik, Universität Rostock, Universitätsplatz 3, 18051 Rostock, Germany*

²⁾*Institute of Computational Technologies SD RAS, Acad. Lavrentjev ave. 6, 630090 Novosibirsk, Russia*

³⁾*Theoretical Quantum Electronics, Technische Universität Darmstadt, 64289 Darmstadt, Germany*

⁴⁾*Institute of Laser Engineering, Osaka University, Osaka 565-0871, Japan*

Among the various attempts to understand collisionless absorption of intense and superintense ultrashort laser pulses a whole variety of models and hypotheses has been invented to describe the laser beam target interaction. In terms of basic physics collisionless absorption is understood now as the interplay of the oscillating laser field with the space charge field produced by it in the plasma. A first approach to this idea is realized in Brunel's model the essence of which consists in the formation of an oscillating charge cloud in the vacuum in front of the target, therefore frequently addressed by the vague term "vacuum heating". The investigation of statistical ensembles of orbits shows that the absorption process is localized at the ion-vacuum interface and in the skin layer: Single electrons enter into resonance with the laser field thereby undergoing a phase shift which causes orbit crossing and braking of Brunel's laminar flow. This anharmonic resonance acts like an attractor for the electrons and leads to the formation of a Maxwellian tail in the electron energy spectrum. Most remarkable results of our investigations are the Brunel like spectral hot electron distribution at the relativistic threshold, the minimum of absorption at $I\lambda^2 \cong (0.3 - 1.2) \times 10^{21} \text{ Wcm}^{-2}\mu\text{m}^2$ in the plasma target with the electron density of $n_e\lambda^2 \sim 10^{23}\text{cm}^{-3}\mu\text{m}^2$, the drastic reduction of the number of hot electrons in this domain and their reappearance in the highly relativistic domain, and strong coupling, beyond expectation, of the fast electron jets with the return current through Cherenkov emission of plasmons. The hot electron energy scaling shows a strong dependence on intensity in the moderately relativistic domain $I\lambda^2 \cong (10^{18} - 10^{20}) \text{ Wcm}^{-2}\mu\text{m}^2$, a scaling in vague accordance with current published estimates in the range $I\lambda^2 \cong (0.14 - 3.5) \times 10^{21} \text{ Wcm}^{-2}\mu\text{m}^2$, and again a distinct power increase beyond $I = 3.5 \times 10^{21} \text{ Wcm}^{-2}\mu\text{m}^2$. The low energy electrons penetrate normally to the target surface, the energetic electrons propagate in laser beam direction.

PACS numbers: 52.38.-r, 52.38.Kd, 52.30.-q, 52.25.Gj, 52.25.Os

I. INTRODUCTION

Intense and superintense laser beam interaction with dense matter is characterized by one prominent phenomenon, that is the generation of superthermal high energy electrons and ions. It leads to the spontaneous question as to the effects that generate them in the absorption process of intense monochromatic light beams. Latest when the kinetic temperature reaches $10^3 Z^2 \text{ eV}$ in the plasma, Z ion charge, collisional absorption is ineffective and other effects of non-collisional nature have to become active in order to ensure absorption. The best known non-collisional candidate so far was resonance absorption at oblique laser incidence^{1,2}. It consists in the direct conversion of laser light into an electron plasma wave resonantly excited at the critical electron density where the laser frequency ω equals the plasma frequency ω_p . High intensity laser pulses in the intensity domain $I = 10^{16} - 10^{22} \text{ Wcm}^{-2}$ with good contrast ratio are so fast rising that there is no time to form a pre-

plasma in front of an irradiated solid sample that could couple to a resonantly excited plasma wave. Therefore the search begun for new collisionless absorption processes. The first successful proposal was the so-called $\mathbf{j} \times \mathbf{B}$ heating³. The authors could show by particle-in-cell (PIC) simulations that at normal incidence the Lorentz force induces non-resonant electron oscillations at 2ω normal to the target surface which lead to appreciable absorption, target heating and production of superthermal electrons at any density above critical. However, no attempt was made to explain how the observed absorption, i.e., irreversibility, comes into play. Not long after a remarkable step forward was made by Brunel⁴ in understanding high-power collisionless absorption. He could show after introducing a few modifications that the resonance absorption concept could be adapted to steep highly overdense plasma profiles and significant absorption could be achieved under oblique incidence despite total absence of plasma resonance at $\omega = \omega_p$ ("not-so-resonant, resonant absorption"⁴) and no possibility for a plasma wave to propagate into a shallow preplasma in front of the target. Instead, now the energy imparted to the electrons is transported into the target and deposited there. Under the assumptions of cold (i) infinitely dense

^{a)} Electronic mail: tatyana.tiseykina@uni-rostock.de

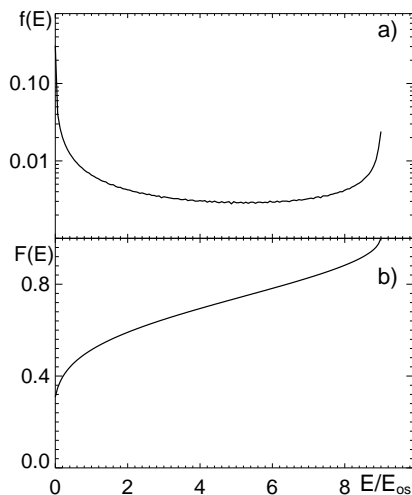


FIG. 1. (a) Electron spectrum $f(E)$ from Brunel's nonrelativistic model⁴; (b) $F(E) = \int f(E') dE'$. Energy E in units of mean oscillation energy in vacuum; energy cut off is at $E = 9.1E_{os}$.

plasma (ii) with discontinuous interface to vacuum (iii) Brunel could formulate the laser-matter interaction dynamics in the vacuum in front of the target in terms of three ordinary differential equations. Perhaps for this reason Brunel's mechanism of the electrons pulled out into the vacuum and then pushed back into the field-free target interior is frequently identified with the term "vacuum heating", an expression coined later for the particles forming a kind of thermal cloud at the vacuum-ion interface in PIC simulations⁵.

To be more specific, the reason why the term vacuum heating played an ominous role in the past and partially still does presently is because, often invoked as the leading collisionless absorption mechanism, it has never been defined properly. To introduce some rating in this respect it seems that two groups of authors can be distinguished. By the concept of vacuum heating the first group addresses the electrons in front of the sharp-edged target that circulate in the vacuum and do not cross the interface during one laser cycle^{5,6}. Identification of vacuum heating with Brunel's mechanism is made by the second group^{7,8} to contrast with anomalous skin layer absorption⁹⁻¹¹. By the latter all motion is strictly confined to the target inside. Sometimes vacuum heating is interpreted as a consequence of unspecified wave breaking^{12,13}. Meanwhile it has been clarified that Brunel/vacuum heating prevails distinctly on skin layer absorption and that vacuum heating in the restricted sense, i.e., the contribution to absorption of the electrons not entering the target with the periodicity of the laser, is almost insignificant¹⁴.

Only recently a detailed analysis and discussion of Brunel's model has been given¹⁵. With a view on the means of the present paper a compact summary of the results may be of interest. The laser field component perpendicular to the target is assumed to have the structure

$E(t) = E_0 \sin \omega t$. It generates electron jets of periodicity $\tau = 2\pi/\omega$. All of them are ejected during the first quarter period and all, except 2.2%, return to the target during the second half period $(\pi, 2\pi)$. During the remaining 3/4 period no further electron ejection is possible as a consequence of partial screening by the outer layers and driver field inversion. Contrary to a common believe that all electrons in one jet are pushed back by the inverted field, only half of them, lifted in the interval $(0, \pi/4)$, are in phase with the driver, the other half experience a weakened driver due to screening and fall back to the target, attracted by the immobile ions, before the laser field has changed direction. This leads quite naturally to a classification into energetic and less energetic electrons. If not specified differently, throughout the paper we define, somehow arbitrarily, those electrons as hot whose return energy exceeds the quiver energy E_{os} of the free electron. Accordingly, 34 % of the Brunel electrons are hot and carry 82 % of the energy in the single jet. In contrast to PIC simulations the Brunel spectrum is non-Maxwellian with a pronounced maximum at $E = 9.1E_{os}$ followed by a sharp cut off (see Fig.1). Absorption $A = I_{abs}/I$ is considerably lower than measured at intermediate angles of incidence¹⁶ but reaches unity at 86° of incidence. A and the absorbed energy scale like $I^{1/2}$ and $I^{3/2}$, respectively. Evidently this is the price Brunel pays for oversimplification. We want to stress that in Brunel's model crossing of layers among each other during the laser action is excluded, except a few front layers whose contribution to absorption is negligible. In other words, the electron flow dynamics is laminar, no wave breaking or, more appropriate in the context, no breaking of flow occurs. Brunel's model offered, within limits, the first physical explanation of $\mathbf{j} \times \mathbf{B}$ heating at 2ω . And yet, Brunel's model does not give a direct physical feeling for the absorption process. The numerous wrong, at least inexact interpretations of it that are still around are a direct indicator (example: "all electrons are pushed back by the laser field" contrasts with the true "free fall" of half of them).

From an early one-dimensional (1D) PIC simulation the energy scaling $E_{hot} \sim I^{1/2}$ has been extracted for the hot electrons¹⁷; it has been re-'confirmed' by independent simulations¹⁸ and apparently by experiments^{19,20}. However, the scaling seems to be questionable for its too strong dependence on intensity; it contrasts with other experiments²¹ and more sophisticated analysis²². In turn, corrections to the latter have been given recently on the basis of a relativistic kinematic model²³. Analogous scaling laws have been proposed by numerous other authors^{16,24-26}. Nevertheless there is no convergence towards a definite scaling²⁷. In order to achieve further progress the investigation has to start from a discussion of collisionless absorption, a flow analysis of the absorbed energy into the various plasma components, a definition of the hot electron component, and completed by analytical modeling in combination with concomitant simulations. In what follows we present our considerations on the degree of understanding collisionless laser

beam absorption, the process of fast electron generation and their interaction with the low electron energy component in order to arrive at more firmly validated scaling relations in forthcoming work. The analysis will enable us also to get insight into shortcomings of the existing models for intense laser-dense matter interaction.

II. COLLISIONLESS ABSORPTION BASICALLY UNDERSTOOD

Let us consider the phenomenon of collisionless absorption of high-power laser beams from a more fundamental point of view. Under quasi-steady state conditions Poynting's theorem averaged over one laser cycle reduces to

$$\overline{\nabla \mathbf{S}} = -\overline{\mathbf{j}\mathbf{E}}. \quad (1)$$

The energy flux density is the Poynting vector $\mathbf{S} = \varepsilon_0 c^2 \mathbf{E} \times \mathbf{B}$; it relates to the laser intensity by $I = \mathbf{S}$. With n_e the electron density and \mathbf{v} the mean electron flow velocity the current density is $\mathbf{j} = -en_e \mathbf{v}$. Equation (1) describes all kinds of absorption, collisional, noncollisional, classical or quantized; in the latter case the current density and the electric field \mathbf{E} are to be substituted by their operators acting on the corresponding state vector $|\psi\rangle$. In the intense laser field, despite the high particle densities involved, the classical picture is an excellent approximation. If the laser field evolves in time as $\mathbf{E} \sim \sin \omega t$ the current density follows as $\mathbf{j} \sim \cos(\omega t + \phi)$ and

$$\overline{\nabla \mathbf{S}} = -\overline{\mathbf{j}\mathbf{E}} \sim -\overline{\cos(\omega t + \phi) \sin \omega t} = -\frac{1}{2} \sin \phi. \quad (2)$$

Dephasing between driver field and current determines the degree of absorption. Thus, collisionless absorption reduces to the problem of finding out which effects lead to a finite phase shift in \mathbf{j} . In collisional absorption it is the friction originating from the collisions between electrons and ions,

$$\overline{\mathbf{j}\mathbf{E}} = \varepsilon_0 \omega_p^2 \frac{\nu}{\omega^2 + \nu^2} |\mathbf{E}|^2 > 0, \quad (3)$$

ν collision frequency. At $\nu = 0$ the collisional phase shift vanishes and any finite ϕ can only be of dynamic origin. Up to $I = 5 \times 10^{20} - 10^{21} \text{ Wcm}^{-2}$ this dynamic origin is found in the space charge induced by $\nabla \mathbf{v} \neq 0$. The space charge generates an electrostatic field that, superposed to the laser field, determines the electron motion and leads to the desired finite phase shift ϕ . This can be seen most immediately with a constant electric field \mathbf{E}_0 . It yields per electron

$$\overline{\mathbf{j}\mathbf{E}} = \frac{2\pi e^2 \mathbf{E}_0^2}{m_e \omega} > 0. \quad (4)$$

It is interesting to note and it can be formally shown, however it is also physically evident that

$\overline{\mathbf{j}(\mathbf{E}_{\text{Laser}} + \mathbf{E}_s)} = \overline{\mathbf{j}\mathbf{E}_{\text{Laser}}}$; all work is done by the driver field, the space charge field \mathbf{E}_s is inert, it provides for the phase shift only. Some authors may attribute absorption to the Brunel like abrupt reduction of the laser wave amplitude in the skin layer. Due to this asymmetry the energy gained by an electron in the vacuum cannot be given back anymore to the wave when entering the evanescent region. However, for this picture to work an electrostatic field component is needed, too; transverse and longitudinal components cannot be isolated from each other. In the standard resonance absorption at the critical density it is the space charge field of the electron plasma wave that provides for collisionless absorption up to 49% through a phase shift $\phi \neq 0$. On the fundamental level of eqs. (2) and (4) collisionless absorption of superintense ultrashort laser pulses may be classified as fully understood now for $I < 10^{21} \text{ Wcm}^{-2}$ for optical wavelengths.

All kinds of difficulties and complications arise when the degree of absorption has to be quantified. This step can only be done by introducing appropriate models. Numerous attempts into this direction have been undertaken with the intention to explain (i) the origin of the hot and the warm electron components, (ii) when and how they are created, during one laser period by direct resonant and nonresonant acceleration, or by stochastic processes over several laser cycles, and (iii) where is absorption localized, in vacuum or in the skin layer. Correspondingly, the existing absorption models may be characterized as statistic or as dynamic. Examples of the first class are vacuum heating in the restricted sense^{28,29}, wave breaking^{12,13}, skin layer absorption, e.g.⁹, linear and nonlinear Landau damping^{30,31}. Candidates of the second class are, first of all, sharp edge absorption⁴, longitudinal³² and transverse³³ ponderomotive heating, "zero vector potential mechanism"¹⁸, relativistic kinematic model²³, anharmonic resonance³⁴. Let our PIC simulations decide on questions (i) - (iii) and to what degree statistics is involved in the dynamics induced by the laser in dense targets.

Now, after three decades of intense studies on superintense laser-matter interaction one would expect that such basic questions (i) - (iii) as labeled above should have found a final answer. The numerous models presented on performed experiments tell the opposite and show that no convergence has been reached yet. It is instructive to have a look at over 100 experimental and theoretical results on the absorption degree collected up to 2009 in³⁵, (Fig. 1 in³⁵), in the irradiance regime from $I\lambda^2 = 10^{18} \text{ Wcm}^{-2} \mu\text{m}^2$, to $10^{21} \text{ Wcm}^{-2} \mu\text{m}^2$. The absorption degrees range from 5% to 95% and yet at the constant irradiance of $6 \times 10^{18} \text{ Wcm}^{-2} \mu\text{m}^2$ absorption between 35% and 85% is reported. It drastically reflects the difficulties encountered in performing unambiguous experiments with all essential parameters well defined. It is this situation that justifies still basic 1D simulations in order to learn more about which are the essential parameters defining the underlying physical processes. For example, a good portion of difficulties and uncertainties

arising in the context of hot electron scaling have their origin in different understanding of when an electron is "hot".

III. LOCALIZATION OF ABSORPTION AND ORIGIN OF FAST ELECTRONS

We consider always linear polarized (in y - direction) laser pulses impinging under 45° angle of incidence onto strongly overdense fully ionized cold hydrogen targets with initial electron density n_{e0} such that $n_{e0}\lambda^2 \simeq 10^{23} \text{ cm}^{-3}\mu\text{m}^2$. The interaction of the laser beam with the target is studied by 1D relativistic PIC simulations using the boost technique³⁶. If not specified differently, throughout the text we call all electrons with energies E exceeding their mean oscillation energy E_{os} "hot" or "fast",

$$E > E_{os} = m_e c^2 [(1 + a^2/2)^{1/2} - 1]; \quad a = \frac{e|\hat{\mathbf{A}}|}{m_e c}$$

$$I\lambda^2 = 1.37 \times 10^{18} a^2 \text{ W/cm}^2 \mu\text{m}^2,$$

$\hat{\mathbf{A}}$ maximum vector potential amplitude.

A. Brunel model and vacuum heating

The energy spectra $f(E)$ of the hot electrons assume the typical shape of Fig.2, here for an $I \sim \sin^4$ laser pulse of full width 50 cycles and $a = 0.3, 1, 3, 10$ after 30, 35, 40, and 50 laser cycles. The straight lines of $\ln f(E)$ starting from the energy E between $2E_{os}/3$ for $a = 10$ and from $E = E_{os}$ for $a \leq 3$ are a clear signature of a Maxwellian type distribution function, $f(E) \sim \exp(-E/k_B T_e)$, k_B Boltzmann constant (for example, the genuine nonrelativistic Maxwellian contains the degeneracy factor \sqrt{E} to be subtracted from $\ln f(E)$ to yield a straight line, see related argument in Sec. V). From the slope an electron "temperature" T_e is determined, with the significance of $k_B T_e$ the mean energy if the straight lines are extrapolated down to $E = 0$. In the Figure T_e is indicated in units of MeV. For $a = 10$ one notices already cooling by energy transfer to the cold electrons and beginning plasma expansion during laser irradiation. Similar hot electron spectra have been reported by other authors, for example by³⁷.

The interaction of intense laser beams with dense targets is very complex and rich of peculiar facets. On the other hand, consequences of basic effects, like collisionless interaction under non-harmonic resonance, are not clarified as they should. Here we report on phenomena which we believe will survive in 2D and 3D also. Let us tentatively identify vacuum heating with the energy gained by all Brunel-like electrons ("Brunel electrons"). It is the sum of energies gained during the excursion into

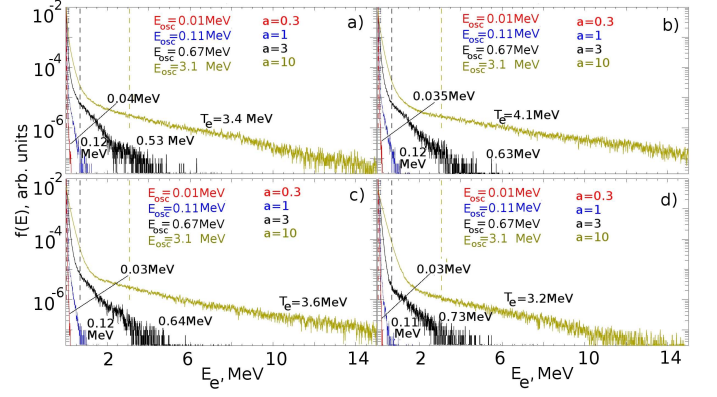


FIG. 2. (Color online) Electron energy spectra $\ln f(E)$ at a) 30, b) 35, c) 40 and d) 45 cycles after the beginning of the interaction. A \sin^4 laser pulse of peak amplitude $a = 0.3, 1, 3, 10$ and full width of 50 cycles impinges under 45° onto a hydrogen target with electron density n_{e0} such that $n_{e0}\lambda^2 = 9 \times 10^{22} \text{ cm}^{-3}\mu\text{m}^2$. The pulses are identical in all four frames. Target thickness varies from 40 to 60 λ . Vertical dashed lines mark the mean oscillation energies. The hot electrons follow a Maxwellian distribution. The maximum mean energies $k_B T_e$ for $a \geq 1$ are by the factors 1.04, 1.09, 1.7 higher than the associated E_{os} . $k_B T_e$ increases during the evolution of laser pulse for $a = 3$, for $a = 10$ it decreases. Power scaling $k_B T_e \sim I^\alpha$, $\alpha \geq 0$ not detected.

vacuum. This energy fraction is identified as "vacuum heating" and compared with the energy absorbed by all electrons. The target thickness is chosen such that no particles are reflected from the target backside and falsify the statistics. The laser beam intensity rises during one laser cycle to its full intensity, is subsequently held constant for 30 cycles and then sinks to zero during another full cycle. In Fig.3 the energies of all Brunel particles and of all particles that have crossed the skin layer at a depth of half a vacuum wavelength are plotted at their crossing time for $a = 1$ and $a = 60$. The salient feature is their jet like structure predicted by the Brunel model. At the low intensity ($a = 1$) there is a clear distinction between the Brunel electrons and all electrons having undergone heating. The increase of the energy maxima from $6.5E_{os}$ to $8E_{os}$ and the more diffuse energy profiles of the jets at half wavelength in depth is a clear indication that some heating is localized in the skin layer, in contrast to the Brunel mechanism. At high intensity ($a = 60$) the jets assume a pronounced double structure due to the increased $\mathbf{v} \times \mathbf{B}$ heating operating at 2ω , but the patterns of the two groups appear equally diffuse. The increase in energy of the fastest electrons is almost no longer visible (increase by $0.5E_{os}$). For $a > 1$ the fraction of Brunel electrons results always higher than the fraction of electrons moving inward and crossing the boundary at $\lambda/2$ in the skin layer. The reason for the difference is to seek in the accumulation of Brunel electrons in the skin layer with increasing laser cycle number, randomized there and repeatedly crossing the target-vacuum

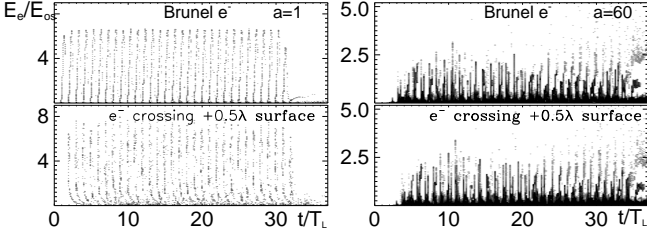


FIG. 3. Energy spectra of Brunel jets (upper pictures) and jets at depth $\lambda/2$ as function of time (units in laser cycles) for $a = 1$ and $a = 60$. Double structure is due to $\mathbf{v} \times \mathbf{B}$ acceleration. Strong reduction of E_{\max}/E_{os} with increasing a is noticeable.

interface before disappearing in the depth of the target. It is instructive to analyze the spectral distribution function $f(E)$ of the Brunel electrons and all electrons just when crossing positions $x = 0.5\lambda, \lambda, 1.5\lambda$ and 2λ for the laser intensities corresponding to $a = 1, 7, 30$ and 60 , see Fig.4. Surprising enough, at low intensity ($a = 1$) and, to a minor degree, also at $a = 7$ the Brunel electrons from the PIC simulations resemble much Brunel's analytical spectrum from Fig.1: The sharp cut offs and the adjacent maxima of $f(E)$ are reproduced, their positions however lie at much lower energies. The maximum of $f(E)$ is still clearly visible for $a = 15$ (not in the Figure), this time at $E = E_{os}$, but the sharp cut off changes into a transition extending over $0.4 E_{os}$. The formation of a Maxwellian tail in the fast electron spectrum occurs in the skin layer and even deeper inside the target. From $a \simeq 20$ on no difference in the spectra from Brunel and total electrons can be observed, they are all "thermalized". At $a = 30$ the spectra extend up to $1.4 E_{os}$, at $a = 60$ the maximum energy is shifted to $E = 3.7 E_{os}$. This is in agreement with the dependence of the fast electron number on laser intensity, see following Section IV.A. From Fig.3 we conclude that at moderate intensities ($a \leq 15$) the skin layer contributes sensitively to the production of the most energetic electrons, either by laser-space charge resonance and/or by stochastic Brunel electron-plasmon interactions.

B. Localization and mechanism of heating

Plasma density and velocity distributions as functions of time are the natural outcome in standard PIC simulations. Additional insight in the heating mechanism is obtained from the orbits $\mathbf{x}(t)$ of randomly chosen electrons. We have analyzed numerous such computer runs each with 200 trajectories stochastically selected from (i) all particles heated by the laser and (ii) from the set of the hot electrons only. In Fig.5 their time histories are depicted for the intensities $a = 7$ (left) and $a = 60$ (right). The salient features characteristic of the two groups are the following:

(1) Heating of the energetic electrons is well localized at

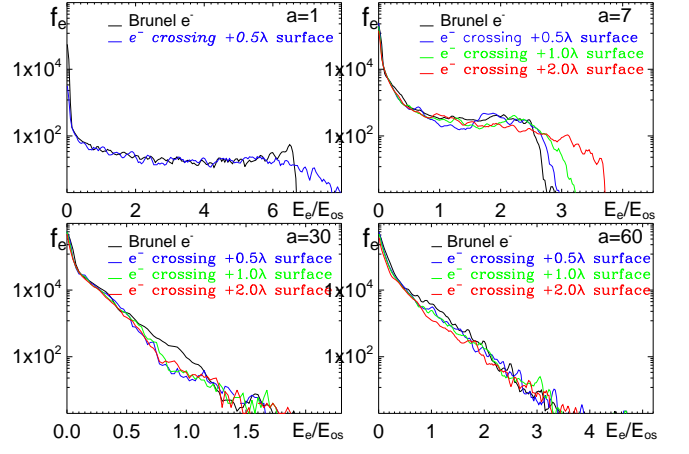


FIG. 4. Energy distributions $f(E)$ of Brunel electrons and of electrons crossing positions $x = 0.5\lambda, 1\lambda, 1.5\lambda$ and 2λ at intensities $a = 1, 7, 30$ and 60 . The distributions are taken after 37 laser cycles when all electrons have returned to position $x = 2\lambda$. The non-Maxwellian structure of the Brunel electrons is preserved up to $a = 15$. For higher intensities there is almost no difference between electrons heated in the vacuum and additional heating in the skin layer region.

the vacuum-target interface and takes place during one laser cycle or a fraction of it. This excludes stochastic heating of the hot electrons. Only a low fraction of them gets the high energy in the skin layer without ever emerging into vacuum.

(2) Contrary to the standard assumption the "slow" return current is highly irregular as a consequence of the interaction of the jets from Fig.3 with the background. It is clearly recognized in Fig.5 that irregular flow sets in just with the arrival of the first jets and it becomes the more irregular the more jets it is exposed to. The jets are accompanied by strong localized electrostatic fields that force electrons from the return current to reverse their direction towards the back of the target or, if they succeed to cross the charge cloud of an incoming jet they are heavily accelerated towards the target front to interact further with the laser field. In short words, the laminar flow of the return current is heavily perturbed by the Cherenkov emission of the plasmons excited by the jets. The stochastic interaction, both, return electron acceleration and deceleration, has been observed in test particle models in the past¹⁴.

(3) The plasma flow in the skin layer breaks (like "wave breaking"), i.e., the orbits cross each other, in contrast to Brunel's laminar model of infinite target density.

(4) Excursion into vacuum ("vacuum heating") of the energetic electrons decreases continuously with a increasing to reach a minimum at around $a = 30$ and then to increase again. Owing to the significance of effects (1) - (3) for localization and understanding hot electron generation, and understanding collisionless laser beam absorption in general, we analyze further the acceleration process. In Brunel's model the density of the target is as-

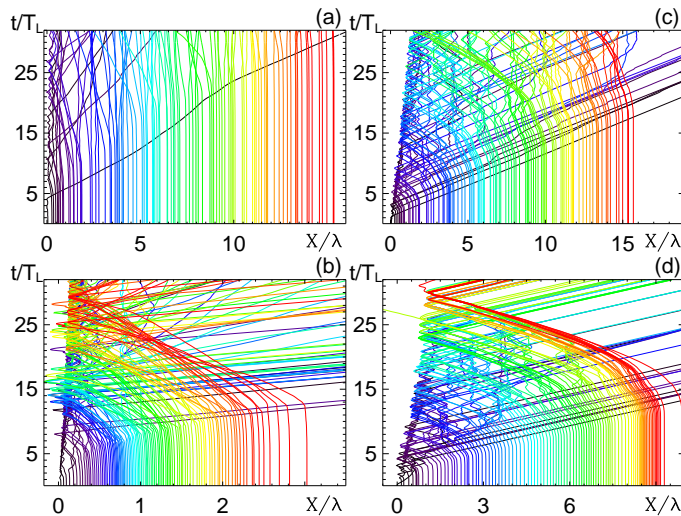


FIG. 5. (Color online) Arbitrary selection of orbits $x_i(t)$, $i = 1 - 100$, for $a = 7$ (a) and $a = 60$ (c). The lower Figures (b) and (d) show the same number of stochastically chosen orbits from the hot electrons only with $E \geq E_{os}$. Their analysis shows acceleration, i.e. heating almost during one laser cycle or a fraction of it in the laser field at the target front and their strong interaction with the return current.

sumed infinite. Consequently all electrons start from the same position and no crossing of orbits occurs, the particle flow into vacuum and back to the target is laminar. Despite Brunel's oversimplification his model explains basic properties of the collisionless interaction: formation of steady state jets (Fig.3), two groups of electron energies (energetic electrons co-moving with the laser field, slow free fall electrons), majority of fast electrons stemming from the excursion into vacuum, dominant fraction of laser energy delivered to hot electrons. If therefore "vacuum heating" is identified with Brunel's mechanism it acquires a precise meaning. However there is the missing link to the physics of acceleration in this simple model. Not to forget that in Brunel's model all heated electrons are lifted into vacuum only during the first quarter laser period. The reality with skin layer included is different: The phase for lifting is stochastic, as expected from broken flow; period doubling, tripling, quadrupling, etc., of electron oscillations occurs in the skin layer (see Fig.5); acceleration to high energies is a resonance effect. To see this we must concentrate once more in detail on single orbits selected statistically. In Fig.6 the time history of four particles starting from different depth in the target together with the electric field (white traces) they "see" during their motion is depicted for $a = 1$, i.e., the orbits $x(t)$ and the momenta $p_x/m_e c$ normal to the target. Resonant interaction in the first 2 pictures is clearly recognized by the abrupt changes in $x(t)$ and $p_x(t)$. Out of resonance the phase difference between field and momentum is $\pi/2$, see $p_x(t)$ and laser field (white line) in the first two pictures. The transition to resonance, i.e. field and momentum antiparallel,

occurs during half a cycle or less in the kink of $x(t)$, seen best by zooming Fig.6. The essential point of this resonance is its anharmonic character. In contrast to the harmonic oscillator in the oscillator with anharmonic potential resonance is an attractor: Given an excitation by the periodic laser above a certain threshold transition to resonance is unavoidable. The reason for this behavior is as follows. The harmonic potential is the only one in which the degree of excitation does not change its periodicity and therefore it either is driven in or out of resonance. The average stochastically perturbed space charge potential of the plasma is flatter than harmonic and so, depending on the excitation level its eigenfrequency changes continuously from the high level ω_p at low excitation down below the laser frequency ω . At the crossing point resonance occurs. It has two consequences: (i) Driver, when in phase with the electron displacement transforms it into a runaway particle in general³⁴; (ii) the resonant phase switch forces the electron to move against the bulk, the plasma flow breaks. Breaking of flow or wave breaking, respectively, often invoked as acceleration or absorption mechanism^{12,13} is never their origin, it is their consequence.

We conclude that at $I < (5 \times 10^{20} - 10^{21}) \text{ Wcm}^{-2}$ the majority of energetic electrons is produced by resonant interaction of the laser field with the longitudinal space charge field over a fraction of one laser cycle in the vacuum as well as in the skin layer. However, there is also indirect acceleration of stochastic nature of the target background, evidenced by the last two pictures in Fig.6 with electrons heated stochastically by the plasmons emanating from the jets. The rapidly oscillating stochastic field of the plasmons increases with the number of jets produced; its influence on stochastic acceleration of electrons is evident in the last two pictures of Fig.6.

IV. FAST ELECTRONS AND ENERGY PARTITION

As seen in the previous section **III** there are several thermalizing mechanism: breaking of flow, skin layer noise, Cherenkov plasmons from jets. As a consequence one would expect that such effects dominate the low energy component of the electrons and that this should propagate mainly normally to the target. The more energetic an electron is the more it feels the Lorentz force in $\mathbf{v} \times \mathbf{B}$ direction forcing its motion into laser beam direction, 45° in this paper. For the single free electron starting from rest in a traveling plane wave the maximum energy gain $\Delta\mathcal{E}$ and the lateral angular spread $\tan\alpha$ of the velocity component v_k in propagation direction to the velocity component in the \mathbf{E} field direction v_E are³⁸

$$\Delta\mathcal{E} = \frac{1}{2}a^2 m_e c^2, \quad \tan\alpha = \left| \frac{v_E}{v_k} \right| = \frac{2}{a}, \quad (5)$$

thus confirming this tendency. In Fig.7 the momenta p_y parallel to the target vs p_x along the target normal of

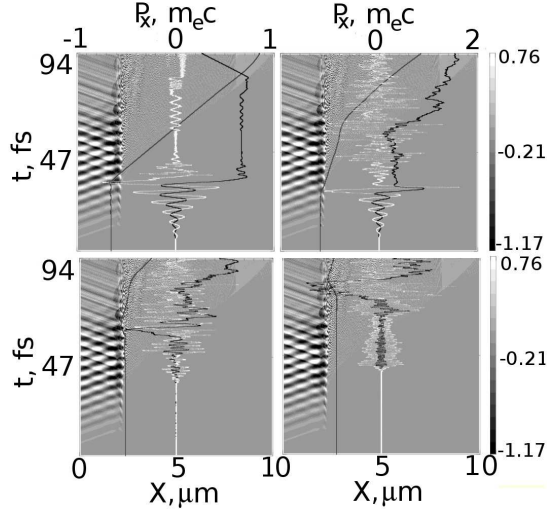


FIG. 6. Anharmonic electron resonance and stochastic interaction³⁴. Regular shadow structure: laser field; black trajectory: orbit $x(t)$ (left) and momentum $p_x(t)$ (right), white traces: electromagnetic/electrostatic field at the particle's position. Primary interaction is by resonance between transverse and longitudinal field during a fraction of laser cycle. Particles in the last two pictures experience stochastic acceleration by plasmons only.

the heated electrons are depicted for $a = 1, 7, 15, 60, 100$. The corresponding distributions of the momenta p_x normal to the target over the space coordinate are shown in Fig.8. From the pictures it is not directly seen that the majority of slow electrons move in the direction of the target normal; however, as expected from (5), with increasing energy the electrons follow indeed the direction of the laser beam. In addition, at $a = 60$ and 100 an appreciable percentage is accelerated into specular direction. The reduction of the absolute number of hot electrons with increasing intensity, their almost vanishing at $a = 15$ and their impressive reappearance towards $a = 100$ is particularly striking. This effect will have direct impact on every attempt to formulate scaling laws for the "hot electron" production. We have counted their number as a function of intensity; the result is reported in Table I. Drop and increase with intensity is beyond expectation.

TABLE I. Number of hot electrons per unit area (arbitrary units) in dependence of a for $n_{e0} = 100n_c = 100m_e\omega^2\epsilon_0/e^2$.

a	1	3	7	15	30	60
N_{hot}	7819	7991	17464	147	265	19273

The formation of spatial spikes within groups of energies and laser intensities is depicted in Fig.8. It has to be seen as complementary to the spike distribution in time in Fig.3. At low laser intensity only the fastest electrons form jets in space as long as they are "young". As they travel further into the target they become in-

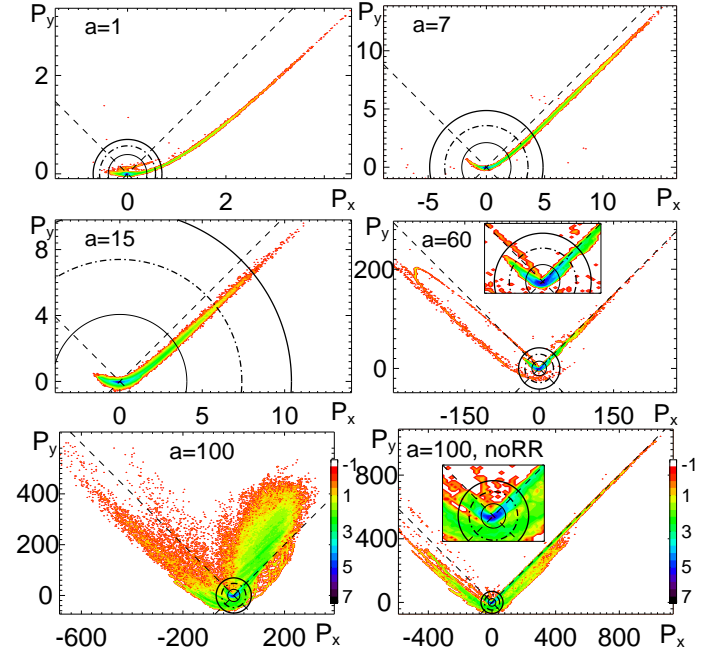


FIG. 7. (Color online) Direction of heated electrons: Momenta $p_y/m_e c$ vs $p_x/m_e c$ for $a = 1, 7, 15, 60$ and 100 (left picture $a = 100$: with radiation damping, right: without) at the end of the standard laser pulse. Electron energies: $E < E_{os}/3$ within inner black circle, $E \in [1/3, 2/3]E_{os}$ within dashed circle, $E \in [2/3, 1]E_{os}$ within bold circle, $E > E_{os}$ ("hot electrons") outside. Circles in the last pictures are very small; therefore see the two insets). The color of the particles in this pictures indicates their number according to the color bar. Low energy electrons within the inner circle (majority in number) penetrate the target normally, energetic electrons follow the laser beam direction (dashed black lines), in $a = 60, 100$ also along the reflected laser beam.

creasingly diffuse as a consequence of their interaction with the Cherenkov plasmons. The electrons of varying velocity undergo mixing in phase space, see uniform background in Figs. 3 and 8, the spikes only are accompanied by strong electrostatic fields. Their damping by friction is given through the collision frequency $\nu_{coll} = 2(e^4 n_{e0} / \epsilon_0 m_e^2 v_e^3 \gamma) \ln \Lambda$. With the Lorentz factor $\gamma = 1, v_e = c$ and $n_{e0} = 10^{23} \text{ cm}^{-3}$ this results in $\nu_{coll} = 5 \times 10^{10} \ln \Lambda \text{ s}^{-1}$, hence, collisional damping of spikes is unimportant. Anomalous interaction of the laser heated electrons with the background has been studied recently³⁹. All electrons after having entered the distinctly relativistic regime show a neat spiky structure because they all fly at light speed and behave much stiffer now against their concomitant space charge field. The inclination of groups of spikes with respect to the normal to the abscissa at subrelativistic speeds is self-explaining. We note also that the excursion of the slow electrons into vacuum (p_x negative) reduces with increasing a .

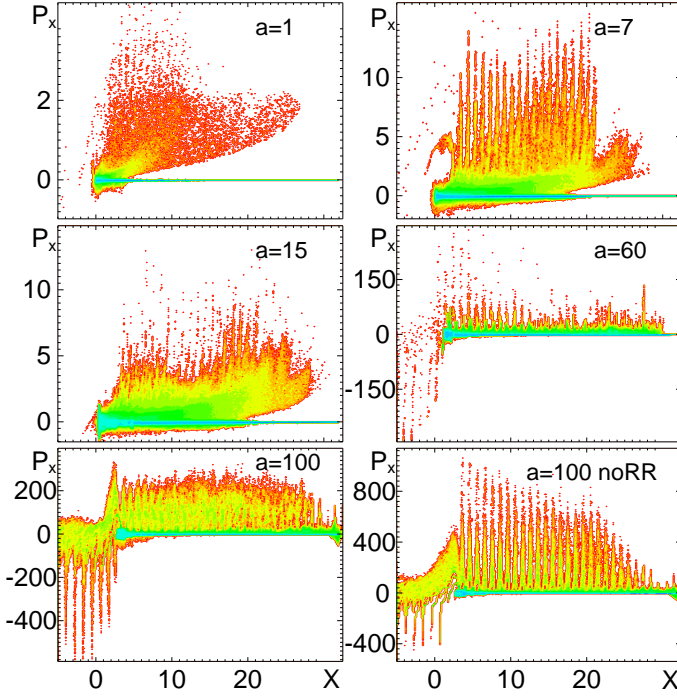


FIG. 8. Energy distribution of heated electrons: Momentum $p_x/m_e c$ vs target normal x for $a = 1, 7, 15, 60$ and 100 (left: with radiation damping, right: without) at the end of the standard laser pulse. The color of the particles indicates their number according to the color bar of Fig. 7. The spiky structure is a rough indicator of relativistic jets.

A. Partition of the absorbed energy

Sometimes it is claimed (at least in the past) that all electrons are "hot" in intense laser-solid target interaction. This rises the question on the percentage of the hot electrons with respect to number, to average energy, or to average flux density. Here, we must stress that a percentage in particle number cannot be given, neither in the experiment nor in the simulation for the simple reason that the fraction depends very sensitively on the total number of particles involved: Where to put the lower threshold? Should the shock heated portion of the target be counted also, or is it reasonable to restrict counting on those electrons that have "seen" the laser at least once? However, the situation is totally different with respect to energy fractions because no ambiguity arises on that. In Table II we present such an absorbed energy partition as a function of laser intensity (parameter $a \sim I^{1/2}$) for two overdense targets, $n_{e0} = 100n_c$ and $n_{e0} = 200n_c$ (for $a = 15$ also $n_{e0} = 400n_c$): overall fraction of absorption I_{abs} ; percentage of energy which is found in the electrons; total fraction of energy absorbed by the hot electrons, $E \geq E_{os}$ and by hot + medium hot electrons of $E > E_{os}/2$ ("warm e^- "); energy fraction transmitted to the ions; energy fraction found in the electrostatic space charge field ("fields"). A first view on the Table tells that the main absorption is accomplished by the ener-

TABLE II. Partition of the incident laser energy: fraction of absorbed intensity I_{abs} transmitted to the electrons, the hot and warm electrons, the ions and the plasmons ("fields") at the end of the standard laser pulse.

a_0	n_{e0}/n_c	A	Energy partition				
			all e^-	hot e^-	warm e^-	ions	fields
0.3	100	0.377	0.25	0.213	0.217	0.009	0.118
	200	0.313	0.24	0.161	0.167	0.007	0.066
0.5	100	0.43	0.28	0.228	0.233	0.01	0.138
1	100	0.358	0.238	0.2	0.211	0.008	0.112
	200	0.354	0.24	0.199	0.206	0.0077	0.106
3	100	0.18	0.122	0.08	0.092	0.003	0.055
	200	0.18	0.123	0.08	0.092	0.003	0.054
5	100	0.2	0.136	0.088	0.102	0.0033	0.061
	200	0.2	0.136	0.089	0.103	0.0026	0.061
7	100	0.19	0.131	0.073	0.089	0.0033	0.056
	200	0.19	0.132	0.076	0.093	0.0025	0.055
15	100	0.067	0.036	0.0002	0.003	0.01	0.021
	200	0.051	0.028	0.0005	0.003	0.007	0.016
	400	0.064	0.039	0.0022	0.008	0.0057	0.019
30	100	0.105	0.0525	0.0002	0.0018	0.0206	0.032
	200	0.045	0.0168	0	0.00012	0.0168	0.011
60	100	0.23	0.126	0.01	0.027	0.033	0.071
	200	0.092	0.031	0.00006	0.0003	0.034	0.027

getic electrons (see 5th and 6th column). The absorption by the ions (protons in the Table) remains modest for $a \leq 15$, however, Cherenkov plasmons ("fields") assume a non negligible portion of laser energy, more than we predicted.

The increase in ion energy beyond $a = 15$ is due to the deeper penetration of the laser as a consequence of the recession of the electrons by the radiation pressure and hence increased energy coupling to the ions.

The overall absorption drops continuously with increasing laser intensity. In contrast to the runaway energy \mathcal{E} in (5) the free quiver energy at fixed oscillation center is $E_{os} = mc^2[\sqrt{1+a^2/2}-1] \sim I^{1/2}$. However this reduction is counterbalanced by the relativistic increase of the critical density, $n_{cr} \sim \gamma n_c$. As the speed of the moderately hot electrons approaches c the absorption into energetic electrons, which is the major portion, should not change; the drop must have a different, non-relativistic origin. Although the scaling of E_{os} and n_{cr} may be oversimplified (see⁴⁰ for n_{cr} scaling) it is correct in its tendency. Our current explanation attributes the very pronounced reduction of absorption to the limiting effect of the electrostatic field on the oscillation amplitude of the single electron: With increasing intensity I the electrons are pushed more and more inward by the radiation pressure. The electron oscillating in the neighborhood of the vacuum-ion interface oscillates in a narrow anharmonic potential the half width of which towards the target interior is a small fraction of the wavelength ("profile steepening"). A similar reduction of absorption has been reported for normal incidence, with an explanation that agrees qualitatively with ours⁴¹. Latest beyond $I \simeq 10^{21} \text{ Wcm}^{-2}$ absorption by the fastest electrons in-

creases again. They are runaway electrons. The electrostatic potential is strong but finite. The phase at which the electrons enter the laser beam is stochastic. Within them there will some of them happen to be in resonance with the field and subject to the Doppler shift

$$\omega' = \gamma(\omega - \mathbf{k}\mathbf{v}), \quad (6)$$

with γ Lorentz factor, \mathbf{k} wave vector. If such an electron is moving inward from the vacuum it sees the incident wave at a Doppler downshifted low frequency and is accelerated over a longer distance whereas the reflected wave is seen at a highly upshifted frequency and represents merely a high frequency disturbance. For an electron moving outward towards the vacuum the accelerating field is that of the reflected wave. The proof of this acceleration mechanism is based on the study of single particle motions, and is directly confirmed by the appearance of energetic electrons flowing into vacuum in the reflected wave direction in the picture for $a = 60$ and $a = 100$ of Fig.7. To give a numerical example of electron displacement lengthening $\Delta x/\lambda$ in a plane TN:SA laser wave ($\lambda = 800$ nm) during a forth cycle $\Delta\varphi = \pi/2$: $\Delta x/\lambda = 3$ at $I = 10^{21}$ Wcm $^{-2}$ and $\Delta x/\lambda = 30$ at 10^{22} Wcm $^{-2}$. For comparison, at $I = 10^{18}$ Wcm $^{-2}$ this shift is 0.03 only. Beyond $I = 10^{22}$ Wcm $^{-2}$ radiation reaction on the electron motion has to be taken into account^{43–45}. A summary of absorption into all plasma channels (electrons, ions, plasmons) its fraction into electrons, the decrease of absorption towards a pronounced minimum close to zero at $a \simeq 15 - 20$ and its rise beyond is presented in Fig.9.

V. ON SCALING LAWS OF THE "HOT ELECTRONS"

From intensity scaling the experimentalist and theoretician expect analytical formulas of the shape of the electron spectrum as a function of the laser intensity. As such a goal seems to be beyond reach at present the high power laser community has limited its focus on the energetic electrons. There, the generation of a Maxwellian tail is one of the characteristics of high power interaction. It is also the most interesting part of the spectrum because, as seen from Table II it contains the main part of the absorbed energy and, last but not least, it is relevant to applications for collective ion acceleration, radiation sources, medical applications, and others. It is aimed at how the number of energetic electrons, the degree of absorption and the mean energy scale with intensity. On the basis of present knowledge scaling of the first two quantities is not feasible. Regarding the mean energy, or the hot temperature $k_B T_{\text{hot}}$, respectively, despite the frequent attempts in experiment and theory no convergence has been achieved so far at all. In the light of our foregoing analysis there is not much surprise about.

The frequently invoked ponderomotive scaling ("Wilks' scaling")¹⁷ of $T_{\text{hot}} \sim I^{1/2}$ is based on the idea that each laser cycle energetic electrons with energy average in the

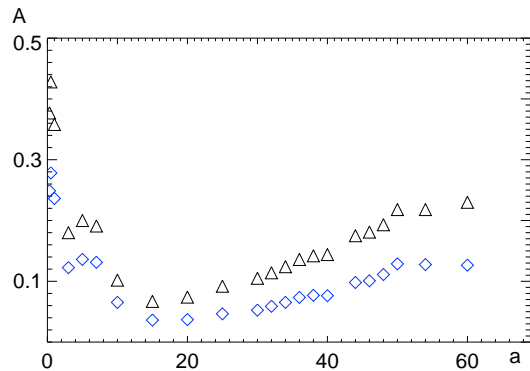


FIG. 9. (Color online) Total absorption (triangles) of a 30 cycles standard laser pulse (see text) and the absorption by electrons (blue diamonds) is given as a function of a . The reduction is due to oscillation inhibition by the induced electrostatic field, its rise beyond is mainly a consequence of entrainment ("runaway electrons").

range of about $E_{\text{os}} = m_e c^2 (\sqrt{1 + a^2/2} - 1)$ are generated. Subsequently this scaling has been recognized as too strong and, in first place guided by experiments²¹, has been replaced by the milder power law⁴⁶ $T_{\text{hot}} \sim I^{0.34-0.4}$ in the intensity range $10^{18} - 10^{21}$ Wcm $^{-2}$. It is intended as to be applied to the unidirectional Maxwellian electrons reaching the analyzer at time $t = \infty$. The search for the right mean energy scaling is equivalent to the search for the process of absorption. In the absence of the stochastic element inherent in collisions it is important to understand whether a Maxwellian tail is one of the signatures of the interaction and, if it is, why.

To arrive at a Maxwellian distribution in an ensemble it is sufficient to know that, given a certain amount of particles n_{hot} containing the amount of energy \mathcal{E}_{hot} , all possible states in the relevant phase space are equally likely and that the Hamiltonian is given by the sum

$$H = \sum_{i=1}^{n_{\text{hot}}} \sqrt{m_e^2 c^4 + c^2 \mathbf{p}_i^2}; \quad |H| = \mathcal{E}_{\text{hot}} \quad (7)$$

which expresses the property that the single electrons are uncorrelated. If the relevant phase space is $\{(\mathbf{p}, \mathbf{q})\}$, as for example in statistical thermodynamics, the resulting distribution is the Maxwellian momentum distribution $f(E) \sim \sqrt{E} \exp(-E/k_B T_{\text{hot}})$, in disagreement with Fig.2. However, as outlined in the foregoing chapters, fast electron generation is by anharmonic resonance. This has the important properties: (i) resonance is an attractor for all electrons above a certain oscillation energy, in contrast to harmonic resonance; the always present crossing of trajectories is a clear indicator of it. (ii) All n_{hot} electrons have the same chance to resonate anharmonically regardless of their phase with respect to the laser driver. This makes it very likely that the relevant phase space is the energy acquired at resonance rather than the momentum. Then from (i) and

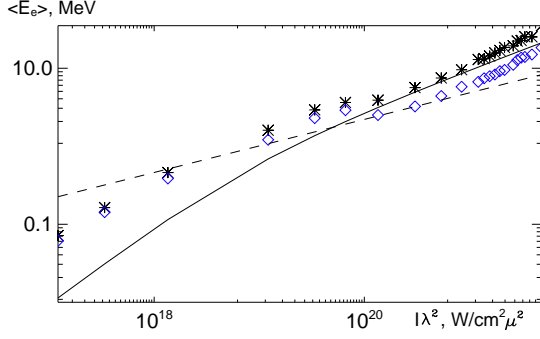


FIG. 10. (Color online) Hot and warm electron energy scaling $\langle E_e \rangle$ with laser intensity $I = 10^{17} - 5 \times 10^{21} \text{ Wcm}^{-2}$, standard pulse. Stars: $E_e \geq E_{os}$ ("hot electrons"); diamonds: $E_e \geq 0.5E_{os}$ ("warm electrons"). In contrast to Fig.2 here $\langle E_e \rangle$ is the average taken over the single energies E_e . Solid line: scaling after⁴², $k_B T_{hot} = m_e c^2 [\sqrt{1 + (I\lambda^2)/(2.74 \times 10^{18})} - 1]$. Dashed line: scaling after²¹, $k_B T_{hot} = m_e c^2 [I\lambda^2/(1.37 \times 10^{18})]^{0.34}$.

(ii) follows that collisionless absorption is accompanied by a Maxwellian tail of energetic electrons (consequence of anharmonic attractor) and the spectrum scales like $f(E) \sim \exp(-E/k_B T_{hot})$, without a degeneracy factor \sqrt{E} . This is what we also deduce from Fig.2.

Let us first examine Fig.2 for pulses $I \sim \sin^4$ in the intensity range $10^{18} - 10^{20} \text{ Wcm}^{-2}$. The uncertainties on the mean energy (slope of log scale) in pictures a) (30 cycles) and c) (40 cycles) are considerable, nevertheless we can conclude with certainty that neither Wilks' original ponderomotive scaling¹⁷ ($I^{0.5}$) nor its improved version are met to some extent. They are far too weak. However, the analysis shows that the assumption $k_B T_{hot} = \kappa \times E_{os}$ with the constant κ not far from unity works. This means that at these relatively low intensities (from $a \simeq 3$ to $a = 10$) the scaling is

$$k_B T_{hot} \sim \sqrt{1 + a^2/2} - 1 \quad (8)$$

in agreement with⁴². From $a = 12$ on E_{os} is well approximated by $m_e c^2 a \sim I^{1/2}$. In Fig.10 we extended the search for scaling from $a = 10$ up to $a = 60$ the latter is already in the runaway regime of absorption. Satisfactory agreement with⁴² is obtained for I from 10^{20} to 10^{21} Wcm^{-2} . Beyond the change in the absorption mechanism and the stiffer coupling to the ions is noticeable in the increase of slope relative to⁴².

VI. SUMMARY AND CONCLUSION

The focus of the present paper is on the physics of collisionless absorption of intense laser beams in dense targets in the intensity domain $I = 10^{18} - 10^{22} \text{ Wcm}^{-2}$ for optical wavelengths, on the variation of the spectral composition of the energetic electrons with intensity and on

their scaling with the latter. Most remarkable results are the Brunel like spectral hot electron distribution at the relativistic threshold, the minimum of absorption at $a \cong 15 - 30$, the drastic reduction of the number of hot electrons in this domain and their reappearance beyond, the strong coupling with the return current beyond expectation, and a strong hot electron scaling in $a \cong 1 - 10$, a scaling in vague accordance with current published estimates in $a \cong 10 - 50$ and a strong increase beyond.

On a fundamental level understanding collisionless absorption is equivalent to the search for the non-orthogonality of induced current density to the laser field. The answer is found in the interplay of the laser field with the space charge field induced by it. The idealized model of Brunel works already on this basis. It is capable of explaining important effects at the relativistic intensity threshold and below, like the generation of two groups of electrons, a hot and a cold component. The non-Maxwellian spectrum predicted by the model is found in our simulations at the relativistic threshold and below; with increasing a it is washed out. By following test orbits we are able to localize absorption at the vacuum-target interface and skin layer for all intensities below the radiation reaction limit at $I \cong 10^{22} \text{ Wcm}^{-2}$ in linear polarization, in agreement with Brunel for non relativistic intensities. If therefore the ominous "vacuum heating" is invoked as responsible for absorption this is correct if it is identified with Brunel's mechanism. What it does not explain, and Brunel does not either, is the underlying physics, i.e. the phase shift and, in concomitance, orbits crossing.

An explanation in terms of physics has to show that (i) such a breaking of flow is not by accident and (ii) a hot Maxwellian tail in the spectrum is a natural outcome from strong drivers. Anharmonic resonance is currently the best model explaining both aspects. It rules stochastic heating and "weave breaking" out automatically. Anharmonic resonance constitutes an attractor (fix point). This kind of resonance always happens in presence of a sufficiently strong driver at any laser frequency and any target density, in contrast to harmonic resonance which is bound to $\omega = \omega_p$. When crossing resonance the momentum of an electron undergoes a phase shift by π or a fraction of it with respect to the bulk of the plasma. Wave breaking, here more appropriately called breaking of flow owing to profile steepening on lengths of a small fraction of a laser wavelength, is a consequence of absorption and energetic electron generation, not its origin.

From $I \cong 5 \times 10^{21} \text{ Wcm}^{-2}$ anharmonic resonance is strengthened by the generation of runaway electrons due to trapping in both, the incident and the reflected laser wave. The reduction up to nearly disappearance of hot electrons $E \geq E_{os}$ is attributed to oscillation inhibition by the ponderomotive space charge field. In the whole intensity domain considered the major fraction of laser energy is deposited in the hot and moderately hot electrons. The next significant portion goes into Cherenkov plasmons excited by the periodic plasma jets. From the

analysis of the test trajectories their coupling to the neutralizing return current is apparent. We consider it as an important aspect when modeling anomalous transport of heat and fast electrons in compressed matter.

Finally, we reexamined the hot electron scaling in 1D, perhaps the most controversially discussed subject in the pertinent literature. Acceptable coincidence with the leading approximations is only found in the intensity range $10^{20} - 10^{21}$. The deviations below $a \cong 10$ are to be attributed mainly to the imprecise proportionality between E_{os} and $I \sim a^2$. In the runaway absorption regime the governing scaling law is still to be discovered. The main reason for the current misunderstandings and disagreements have to be attributed to the poor knowledge of the electron energy spectrum $f(E)$. What is missing most at present in the experiment and in the theory is a clear definition of what means "hot" and "cold" electrons. In order not to fall into this deficiency we define electrons as "hot" and "moderately hot" if their energy is higher than E_{os} and $(0.5 - 2/3)E_{os}$. It is approximately the range of the Maxwellian tail. The commonly used terminology "Maxwellian" is misleading because it refers to the electron velocities \mathbf{v} or momenta with a distribution law $df(E) = v^2 \exp(-E/k_B T_{hot}) dv \sim \sqrt{E} \exp(-E/k_B T_{hot}) dE$. This differs from our findings (and, implicitly, others) of a Boltzmann distribution $df(E) = \exp(-E/k_B T_{hot}) dE$ for the relevant restricted phase space of total energies $\mathcal{E} = \sum E_i$.

ACKNOWLEDGMENTS

This work was in part supported by the DFG within the SFB 652. PIC simulations were performed using the computing resources granted by the John von Neumann-Institut für Computing (Research Center Jülich) under the project HRO01. We gratefully thank Dr. Andrea Macchi (University of Pisa, Italy) for providing us his 1D PIC code and Prof. Su-Ming Weng (Jiao Tong University, Shanghai) for his contributions of ideas and suggestions. The continuous support of this work by Prof. Dieter Bauer (University of Rostock, Germany) is gratefully acknowledged.

¹A. D. Piliya, Sov. Phys. Tech. Phys. **11**, 609 (1966).

²H.-J. Kull, Phys. Fluids **26**, 1881 (1983).

³W. L. Kruer, K. Estabrook, Phys. Fluids **28**, 430 (1985).

⁴F. Brunel, Phys. Rev. Lett. **59**, 52 (1987); Phys. Fluids **31**, 2714 (1988).

⁵P. Gibbon, A. R. Bell, Phys. Rev. Lett. **68**, 1535 (1992).

⁶P. Gibbon, Phys. Rev. Lett. **73**, 664 (1994).

⁷L. M. Chen, J. Zhang, Q. L. Dong, H. Teng, T. J. Liang, L. Z. Zhao, and Z. Y. Wei, Phys. Plasmas **8**, 2925 (2001); Q. Dong and J. Zhang, Science in China **46**, 71 (2003); D. Umstadter, J. Phys. D **36**, R151 (2003); S. Kato, J. Plasma Fusion Res. **6**, 658 (2004).

⁸A. V. Getz and V. P. Krainov, J. Exp. Theor. Phys. **101**, 80 (2005).

⁹W. Rozmus and V. T. Tikhonchuk, Phys. Rev. A **42**, 7401 (1990); W. Rozmus, V. T. Tikhonchuk, and R. Cauble, Phys. Plasmas **3**, 360 (1996).

- ¹⁰T.-Y. B. Yang, W. L. Kruer, R. M. More, and A. B. Langdon, Phys. Plasmas **2**, 3146 (1995); T.-Y. B. Yang, W. L. Kruer, A. B. Langdon, and T. W. Johnston, Phys. Plasmas **3**, 2702 (1996).
- ¹¹G. Ferrante, M. Zarcane, and S. A. Uryupin, Phys. Plasmas **9**, 4560 (2002).
- ¹²S. Kato, B. Bhattacharyya, A. Nishiguchi and K. Mima, Phys. Fluids B **5**, 564 (1993).
- ¹³H.-B. Cai, Phys. Plasmas **13**, 063108 (2006).
- ¹⁴D. Bauer and P. Mulser, Phys. Plasmas **14**, 023301 (2007).
- ¹⁵P. Mulser, S.-M. Weng, and T. Liseykina, Phys. Plasmas **19**, 043301 (2012).
- ¹⁶M. Cerchez, R. Jung, J. Osterholz, T. Toncian, O. Willi, P. Mulser, and H. Ruhl, Phys. Rev. Lett. **100**, 245001 (2008).
- ¹⁷S. C. Wilks, W. L. Kruer, M. Tabak, and A. B. Langdon, Phys. Rev. Lett. **69**, 1383 (1992).
- ¹⁸T. Baeva, S. Gordienko, A. P. L. Robinson, P. A. Norreys, Phys. Plasmas **18**, 056702 (2011).
- ¹⁹G. Malka and J. L. Miquel, Phys. Rev. Lett. **77**, 7578 (1996).
- ²⁰P. McKenna, F. Lindau, O. Lundh, D. C. Carroll, R. J. Clarke, K. W. D. Ledingham, T. McCanny, D. Neely, A. P. L. Robinson, L. Robson, P. T. Simpson, C.-G. Wahlström, and M. Zepf, Plasma Phys. Control. Fusion **49**, B223 (2007).
- ²¹F. N. Beg, A. R. Bell, A. E. Dangor, C. N. Danson, A. P. Fews, M. E. Glinsky, B. A. Hammel, P. Lee, P. A. Norreys, and M. Tatarakis, Phys. Plasmas **4**, 447 (1997).
- ²²M. G. Haines, M. S. Wei, F. N. Beg, and R. B. Stephens, Phys. Rev. Lett. **102**, 045008 (2009).
- ²³P. Gibbon, A. A. Andreev, and K. Yu. Platonov, Plasma Phys. Control. Fusion **54**, 045001 (2012).
- ²⁴C. D. Chen, J. A. King, M. H. Key, K. U. Akli, F. N. Beg, H. Chen, R. R. Freeman, A. Link, A. J. Mackinnon, A. G. MacPhee, P. K. Patel, M. Porkolab, R. B. Stephens, and L. D. Van Woerkom, Rev. Sci. Instrum. **79**, 10E305 (2008).
- ²⁵A. G. MacPhee, K. U. Akli, F. N. Beg, C. D. Chen, H. Chen, R. Clarke, D. S. Hey, R. R. Freeman, A. J. Kemp, M. H. Key, J. A. King, S. Le Pape, A. Link, T. Y. Ma, H. Nakamura, D. T. Offermann, V. M. Ovchinnikov, P. K. Patel, T. W. Phillips, R. B. Stephens, R. Town, Y. Y. Tsui, M. S. Wei, L. D. Van Woerkom, and A. J. Mackinnon, Rev. Sci. Instrum. **79**, 10F302 (2008).
- ²⁶T. Kluge, T. Cowan, A. Debus, U. Schramm, K. Zeil, and M. Bussmann, Phys. Rev. Lett. **107**, 205003 (2011).
- ²⁷A. Macchi, *A Superintense Laser-Plasma Interaction Theory Primer* (Springer New York, 2013), Chap. 4, Sec. 2.
- ²⁸Y. Sentoku, V. Y. Bychenkov, K. Flippo, A. Maksimchuk, K. Mima, G. Mourou, Z. M. Sheng, and D. Umstadter, Appl. Phys. B **74**, 207 (2002).
- ²⁹V. S. Rastunkov, V. P. Krainov, Laser Phys. **15**, 262 (2005).
- ³⁰D. F. Zaretsky, Ph. A. Korneev, S. V. Popruzhenko, and W. Becker, J. Phys. B **37**, 4817 (2004).
- ³¹Ph. A. Korneev, S. V. Popruzhenko, D. F. Zaretsky, and W. Becker, Laser Phys. Lett. **2**, 452 (2005).
- ³²A. V. Sofronov and V. P. Krainov, J. Phys. B **37**, L329 (2004).
- ³³A. Pukhov, Rep. Prog. Phys. **66**, 47 (2003).
- ³⁴P. Mulser, D. Bauer, and H. Ruhl, Phys. Rev. Lett. **101**, 225002 (2008).
- ³⁵J. R. Davies, Plasma Phys. Control. Fusion **51**, 014006 (2009). Nucl. Instrum. Methods Phys. Res. A **544**, 61 (2005).
- ³⁶P. Gibbon, A. A. Andreev, E. Lefebvre, G. Bonnaud, H. Ruhl, J. Delettrez, and A. R. Bell, Phys. of Plasmas **6**, 947 (1999).
- ³⁷A. J. Kemp, Y. Sentoku, and M. Tabak, Phys. Rev. E **79**, 066406 (2009).
- ³⁸P. Mulser and D. Bauer, *High Power Laser-Matter Interaction* (Springer Heidelberg, 2010), p. 356.
- ³⁹M. Sherlock, E. G. Hill, R. G. Evans, and S. J. Rose, Phys. Rev. Lett. **113**, 255001 (2014).
- ⁴⁰S. M. Weng, P. Mulser, and Z. M. Sheng, Phys. Plasmas **19**, 022705 (2012).
- ⁴¹J. Sanz, A. Debayle, and K. Mima, Phys. Rev. E **85**, 046411 (2012).
- ⁴²H. Chen, S. C. Wilks, W. Kruer, P. Patel, and R. Shepherd,

- Phys. Plasmas **16**, 020705 (2009).
- ⁴³N. Naumova, T. Schlegel, V. T. Tikhonchuk, C. Labaune, I. V. Sokolov, and G. Mourou, Phys. Rev. Lett. **102**, 025002 (2009).
- ⁴⁴M. Tamburini, T.V. Liseykina, F. Pegoraro, and A. Macchi, Phys.Rev. E **85**, 016407 (2012); M. Tamburini, F. Pegoraro, A. Di Piazza, C. H. Keitel, and A. Macchi, New J. Phys. **12**, 123005 (2010).
- ⁴⁵L. L. Ji, A. Pukhov, I. Yu. Kostyukov, B. F. Shen, and K. Akli, Phys. Rev.Lett **112**, 145003 (2014).
- ⁴⁶S. C. Wilks and W. L. Kruer, IEEE J. of Quantum Electronics, **33**, 1954 (1997).